RESEARCH ON TRANSMISSION PERFORMANCE AND EXPERIMENT OF OUTER CAGE MAGNETIC COUPLING

Junyue YANG[1], Daming WANG[2], Yanjun GE[3]

In order to improve operation efficiency and heat dissipation capacity of magnetic coupling, an outer cage magnetic coupling was proposed by combining structure of permanent magnet motor and asynchronous motor. According to principle of equivalent magnetic circuit and equivalent circuit, electromagnetic torque equation was obtained, then heat dissipation structure was designed and heat flow field was analyzed. Based on theoretical analysis, a 37kW experimental prototype was designed and manufactured, transmission performance and temperature rise experiments were carried out to verify correctness and feasibility of the theoretical analysis.

Keywords: Magnetic coupling; Outer cage rotor; Transmission performance; Heat dissipation structure.

1. Introduction

Magnetic coupling is a new permanent magnet transmission device, which realizes contactless torque transmission by magnetic field coupling, it can replace hydraulic coupling and frequency converter to realize stepless speed regulation in application of centrifugal load machinery, it also has advantages of high reliability, non-contact, non-polluting, cushioning, shock absorption, and has broad application prospects.[1] [2] [3] [4] [5]

According to structure of conductor rotor, magnetic coupling can be divided into solid rotor type and cage rotor type. The solid rotor has large eddy current loss and obvious skin effect in working process, which reduces the transmission efficiency.[6][7][8][9] In reference [10], Yanjun GE proposed a magnetic coupling based on cage rotor of asynchronous motor, which has advantages of simple structure, low cost, and small eddy current loss. However, in this structure, squirrel cage rotor as inner rotor is not conducive to heat dissipation, limited in application of high-power system.

Therefore, this paper proposes a magnetic coupling structure of outer cage rotor, which is conducive to high-power transmission and air-cooled heat

[1] Lect. , Dalian Jiaotong University, Dalian, China, e-mail:xyk40@126.com
[2] Ph.D. candidate , Dalian Jiaotong University, Dalian, China, e-mail: wangdaming1987@163.com
[3] Prof., Dalian Jiaotong University, Dalian, China, e-mail: geyanjun1964@126.com

dissipation on the basis of ensuring electromagnetic torque and speed regulation performance.

2. Structure and principle

Outer cage magnetic coupling is composed of conductor rotor (outer rotor), air gap and permanent magnet rotor (inner rotor), as shown in Fig. 1. The structure of outer rotor is similar to that of squirrel cage rotor of asynchronous motor, which is composed of cage conductor structure and iron core. As inner rotor, permanent magnet rotor is composed of inner rotor core and permanent magnet blocks, the permanent magnet blocks are evenly embedded in inner rotor core along circumferential direction in form of alternating arrangement of N and S poles. There is a uniform air gap between inner and outer rotor.

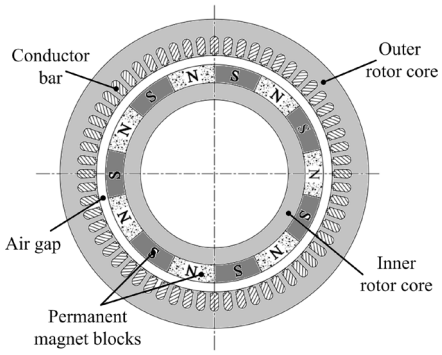

Fig. 1 Basic structure

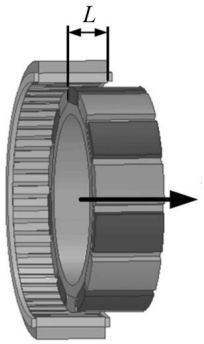

Fig. 2 Adjustable-speed sketch

At runtime, a relative slip is formed between inner and outer rotor, magnetic field generated by permanent magnet blocks cut cage conductor bars, resulting in induced current and electromagnetic torque.

By adjusting axial coupling length L of inner and outer rotor, effective area of magnetic field is changed, so as to adjust slip and realize stepless speed regulation, as shown in Fig. 2.

3. Magnetic field analysis and electromagnetic torque calculation

In Fig. 1, structure of inner rotor is similar to rotor of surface-mount permanent magnet motor, which can be analyzed by equivalent magnetic circuit method. The permanent magnet is equivalent to a magnetomotive force source.

$$F_c = H_c h_c \tag{1}$$

Where, F_c is calculated magnetomotive force of permanent magnet source, H_c is coercivity of permanent magnet, and h_c is length of permanent magnet in magnetization direction.

The equivalent magnetic circuit is shown in Fig. 3.

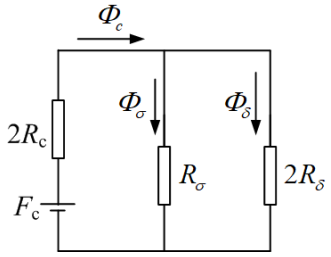

Fig. 3 Equivalent magnetic circuit

In Fig. 3, Φ_c is total flux of permanent magnet, Φ_σ is flux leakage, Φ_δ is main flux of air gap, R_c is permanent magnet block magnetoresistance, R_σ is flux leakage reluctance, and R_δ is air gap reluctance.

$$R_c = \frac{h_c}{\mu_0 \mu_c S} \tag{2}$$

$$R_\delta = \frac{\delta}{\mu_0 S} \tag{3}$$

Where, μ_0 is permeability of vacuum, μ_c is relative permeability of permanent magnet, S is effective magnetic flux area and δ is air gap length.

Ignoring flux leakage effect, simplified magnetic circuit equation can be expressed as follows.

$$F_c = \Phi_\delta (2R_c + 2R_\delta) \tag{4}$$

$$\Phi_\delta = \frac{\mu_0 \mu_c F_c S}{2(h_c + \mu_c \delta)} \tag{5}$$

Then air gap magnetic density B'_δ can be expressed as Eq. (6).

$$B'_\delta = \frac{\Phi_\delta}{S} = \frac{\Phi_\delta}{\pi d L} \tag{6}$$

Where, d is outer diameter of inner rotor.

If inner rotor rotates at angular speed ω_0, fundamental wave distribution of air gap magnetic field along circumference can be obtained by Fourier expansion, as shown in Eq. (7).

$$b_\delta(\theta, t) = B_\delta \cos(p\theta - \omega_0 t) \tag{7}$$

Where, p is number of permanent magnet pole pairs, θ is circumferential angle, t is time, and B_δ is fundamental amplitude of air gap magnetic density.

$$B_\delta = \frac{4}{\pi} B'_\delta \tag{8}$$

At runtime, there is a slip between inner and outer rotor, and slip rate s can be expressed as Eq. (9).

$$\frac{\omega_0 - \omega_1}{\omega_0} = s \tag{9}$$

Where, ω_1 is rotation angular velocity of outer rotor, and $\omega_0 \geqslant \omega_1$.

Outer rotor circuit is induced by magnetic field rotation of inner rotor, which can be analyzed by equivalent circuit method of asynchronous motor, as shown in Fig. 4.

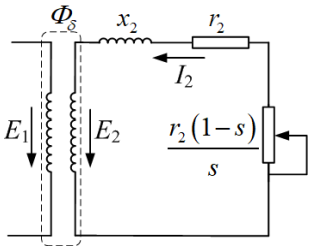

Fig. 4 Equivalent circuit

In Fig. 4, E_1 is equivalent electromotive force of inner rotor, E_2 is equivalent electromotive force of outer rotor, I_2 is equivalent current of outer rotor, r_2 is equivalent resistance of outer rotor, and x_2 is equivalent leakage reactance of outer rotor when slip is 1. According to equivalent circuit conversion principle, potential balance equation can be shown as Eq. (10).

$$E_1 = E_2 = \frac{d\Phi_\delta}{dt} = I_2\left(\frac{r_2}{s} + jx_2\right) \tag{10}$$

The cage conductor in outer rotor is equivalent to a symmetrical polyphase winding. Each conductor bar is equivalent to one phase winding, and induced electromotive force of each conductor bar can be expressed as Eq. (11).

$$e_{2i} = b_\delta(\theta, \ t)\omega_0 dL/2 \tag{11}$$

Induced current of each conductor bar can be expressed as Eq. (12).

$$i'_{2i} = \frac{e_{2i}}{\frac{r'_2}{s} + jx'_2} \tag{12}$$

Where, i'_{2i} is induced current of each conductor bar, r'_2 is equivalent resistance of conductor bar, and x'_2 is equivalent leakage reactance of conductor bar when slip rate is 1.

Then electromagnetic power P_1 transmitted by air gap can be expressed as Eq. (13).

$$P_1 = \sum_{k=1}^{z} e_{2k} i'_{2k} = \sum_{i=k}^{z} e_{2k} i_{2k} \cos\varphi_2 \tag{13}$$

Where, z is number of cage rotor conductor bars, i_{2k} is effective current value of each conductor bar.

$$i_{2k} = \frac{e_{2k}}{\sqrt{\left(\frac{r_2'}{s}\right)^2 + x_2'^2}} \tag{14}$$

And $\cos\varphi_2$ is power factor of outer rotor.

$$\cos\varphi_2 = \frac{sr_2'}{\sqrt{r'^2 + \left(sx_2'\right)^2}} \tag{15}$$

The current in conductor bar can be converted to inner surface of outer cage rotor [10], and electromagnetic torque T_e can be expressed as Eq. (16).

$$T_e = \frac{P_1}{\omega_1} = \frac{2\pi^2 d^2 B_\delta^2 L^2 s r_2'}{\omega_0 \left[r_2'^2 + (sx_2')^2 \right]} \tag{16}$$

Analysis Eq. (16), stepless speed regulation can be realized by adjusting axial coupling length L.

According to similarity theoretical formula of centrifugal load, in process of centrifugal load speed regulation, load torque is directly proportional to square of speed, as shown in Eq. (17).

$$T_e = T_N (1-s)^2 \tag{17}$$

Where, T_N is rated torque of centrifugal load.

At runtime, losses include hysteresis loss, eddy current loss of cores, current loss and mechanical loss (bearing friction, wind resistance, etc.), in which current loss is main heat source, according to Eq. (17), current loss P_Ω can be expressed as Eq. (18).

$$P_\Omega = \sum_{k=1}^{z} i_{2k}^2 r_2' = P_N s (1-s)^2 \tag{18}$$

Where, P_N is rated power of centrifugal load.

According to Eq. (18), when slip rate is 1/3, the maximum current loss is 4/27 of rated load power. This state is also reference point for design of heat dissipation system.

4. Design and development of prototype

Based on theoretical analysis, a 37kW experimental prototype is designed, input speed is 1500rpm and rated electromagnetic torque is 239Nm. Structural parameters are shown in Table 1.

Table 1

Structural parameters of experimental prototype

Parameter	Value
Pole pairs of permanent magnet	7

Width of permanent magnet(mm)	42
Length of permanent magnet(mm)	56
Thickness of permanent magnet (mm)	15
Outer yoke thickness (mm)	20
Air gap length (mm)	3
Outer diameter of inner rotor (mm)	230
Inner diameter of outer rotor (mm)	236
outer diameter of outer rotor (mm)	280
Number of rotor slots	60
Material of permanent magnet	N35NdFeB
Material of conductor bar	Cast aluminum
Material of outer rotor core	Q235
Material of inner rotor core	Q235

Considering difficulty of processing technology, permanent magnet block is a combination structure of trapezoidal and circular arc, and magnetization mode is parallel magnetization. Slot type of outer rotor is pyriform, which avoids accumulation of magnetic lines and sharp angle effect. The detailed structure of permanent magnet block (mm) and outer rotor slot (mm) are shown in Fig. 5.

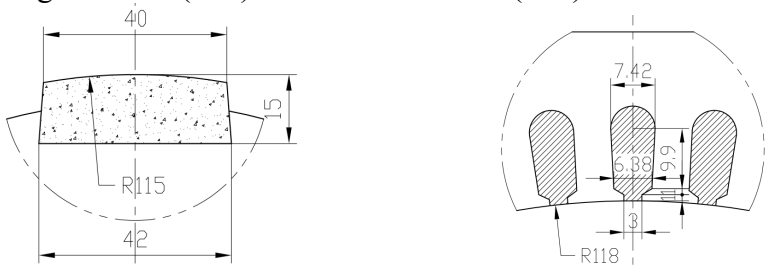

(a) Structure of permanent magnet block (b) Structure of outer rotor slot

Fig. 5 Detailed structure of permanent magnet block and outer rotor slot

The structure of experimental prototype is shown in Fig. 6.

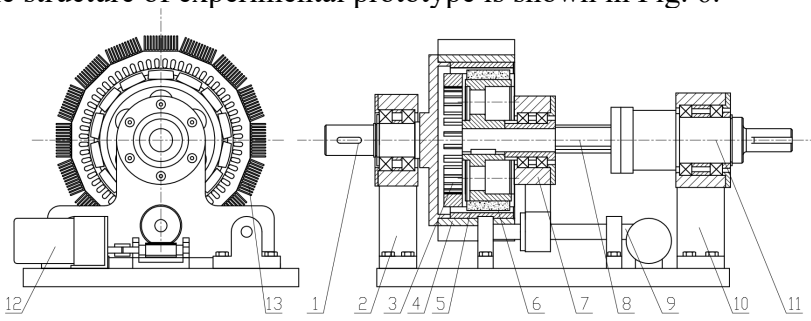

Fig. 6 Structure of experimental prototype

1. Input shaft, 2. Bearing pedestal of input end, 3. Shaft end blades, 4. Outer rotor core, 5. Conductor bar, 6. Permanent magnet block, 7. Movable bearing pedestal, 8. Ball spline, 9. Guide rod, 10. Bearing pedestal of output end, 11. Output shaft, 12. Motor of speed regulating mechanism, 13. Heat dissipation fins.

In Fig. 6, design objective of heat dissipation system mainly includes increasing heat dissipation area and increasing air flow rate. Installing heat dissipation fins on outer surface of outer rotor can effectively increase heat dissipation area, improve air disturbance degree of whole flow field and enhance convective heat transfer, as shown in Fig. 7.

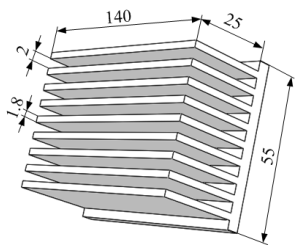

Fig. 7 Heat dissipation fins

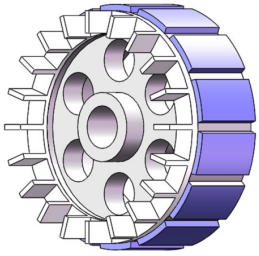

Fig. 8 Shaft end blades

Shaft end blades are installed on side end face of inner rotor to enhance air flow on surface, break air retention dead zone and improve convective heat transfer efficiency, as shown in Fig. 8.

Thermal process analysis model of prototype is established in SolidWorks. According to equation (18), taking heating condition with slip rate 1/3 as analysis point, differential equation of simulated temperature field can be shown as Eq. (19).

$$\frac{\partial}{\partial x}\left(\lambda_x \frac{\partial T}{\partial x}\right)+\frac{\partial}{\partial y}\left(\lambda_y \frac{\partial T}{\partial y}\right)+\frac{\partial}{\partial z}\left(\lambda_z \frac{\partial T}{\partial z}\right)+q=0 \tag{19}$$

Where, λ_x, λ_y, λ_z are components of thermal conductivity in x, y, z direction, T is temperature of object, q is heat flux density of object.

Three kinds of boundary conditions are set for each component in model: temperature on boundary of object, temperature change rate in normal direction of boundary between object and air, relationship between change rate of object temperature at boundary and convective heat transfer on boundary surface, as shown in Eq. (20).

$$\left.\begin{aligned} T_w &= T_0 \\ -\lambda\frac{\partial T}{\partial n} &= q_0 \\ -\lambda\frac{\partial T}{\partial n} &= h\left(T_w - T_f\right) \end{aligned}\right\} \tag{20}$$

Where, T_w is average temperature of object surface, T_0, q_0, T_f are constants related to materials, λ is thermal conductivity.

Thermal properties of main parts at 20 ℃ is shown in Table 2.

Table 2

Thermal properties of main parts

Parts	Material	Thermal conductivity [W/(m·K)]	Material density kg/m^3	Specific heat capacity [J/(kg▪ ℃)]
Inner rotor core	Q235	50	7.8×10^3	460
Conductor bar	Cast aluminum	217.7	2.7×10^3	880
Permanent magnet	N35NdFeB	7.7	7.5×10^3	465
Outer rotor core	Q235	50	7.8×10^3	460
Heat dissipation fins	Al6063	201	2.7×10^3	880
Air gap	Air	0.1	1.29	1007

The 3-D heat flow field of model can be analyzed in Flow Simulation module, analysis type is internal, physical characteristic is internal heat conduction of solid, fluid is air, initial temperature is 40℃, and adaptive mesh generation method is adopted in calculation process.

In Fig. 9, air flow trace can be drawn by finite element analysis method. By action of heat dissipation system, internal air flow speed reaches 15m/s, forming a smooth wind path.

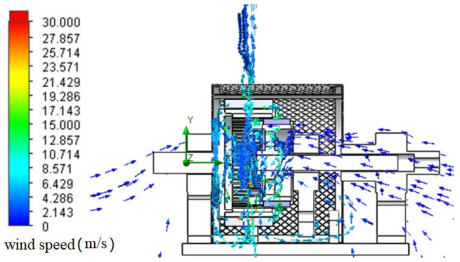

Fig. 9 Flow trace of prototype

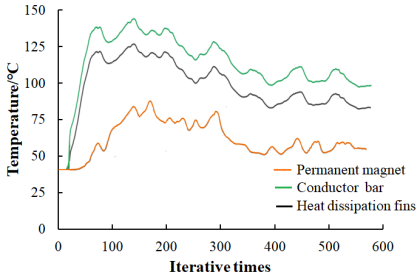

Fig.10 Temperature convergence curve

Temperature rise calculation results of main parts are shown in Fig. 10. After 600 iterations, temperature of permanent magnet converges to 54℃, temperature of conductor bars converges to 102℃, and temperature of heat dissipation fins converges to 87℃, all lower than allowable temperature of material, which proves rationality of heat dissipation system.

The assembly of prototype and main parts are shown in Fig. 11.

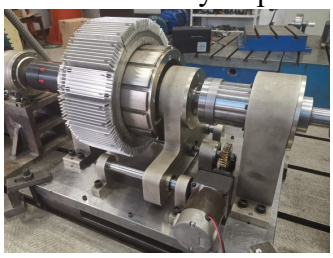

(a) Assembly of prototype

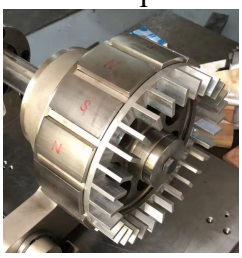

(b) Inner rotor

(c) Outer rotor

Fig. 11 Assembly of prototype and main parts

5. Experiment and result analysis

In Fig. 12, experimental platform mainly includes: driving motor (YP2-280-4M), torque sensor 1, torque sensor 2 (model: JD20, range: 0~1000Nm, accuracy: 0.2%), and loading motor (YP2-280-4M).

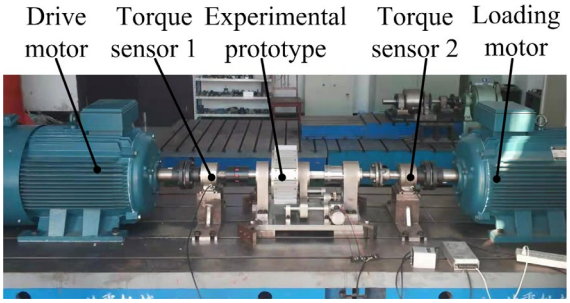

Fig. 12 Experimental platform

The driving motor speed is 1500rpm, and relationship between electromagnetic torque and output speed in total coupled state can be obtained by loading experiment, which is compared with theoretical curve, as shown in Fig. 13.

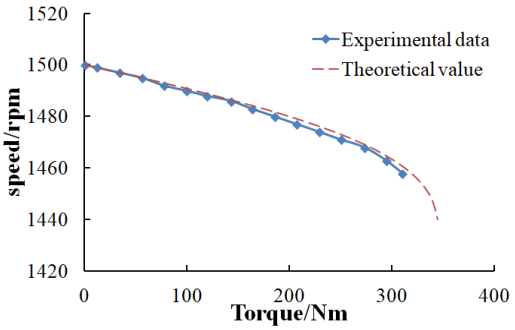

Fig. 13 Relationship between torque and speed in total coupled state

In Fig. 13, the maximum loading torque is 310Nm, which is 1.3 times of rated torque of design (239Nm), experimental prototype still works in linear area, and experimental data are uniform with theoretical curve. Error of each measurement point is within 3%. The comparison results show correctness of theoretical calculation.

In Fig. 13, experimental prototype shows relatively hard mechanical characteristic, and its slip rate is only 0.019 under condition of rated torque. Electromagnetic torque density is 69kNm/m^3, which is much higher than that of asynchronous motor with same capacity (10~30kNm/m^3), so operation efficiency of air gap magnetic field is greatly improved.

By adjusting coupling length, mechanical characteristic curves of different coupling lengths can be obtained. As shown in Fig. 14, there are mechanical

characteristic curves of 26mm and 11mm coupling length, which are compared with corresponding theoretical curves.

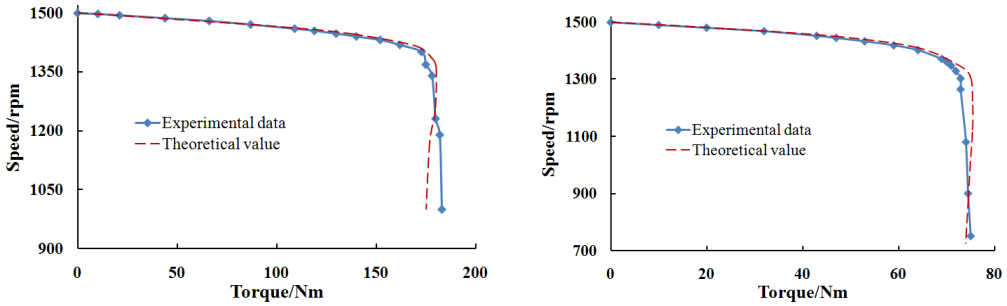

(a) 26mm coupling length (b) 11mm coupling length

Fig. 14 Mechanical characteristic curves of different coupling lengths

In Fig. 14, experimental data of different coupling lengths are still uniform with corresponding theoretical curve, error of each measurement point is within 5%.

For different coupling lengths, a family of mechanical characteristic curves can be got, which intersect with speed regulating curve of centrifugal load, each intersection is working point of speed regulating process, as shown in Fig. 15.

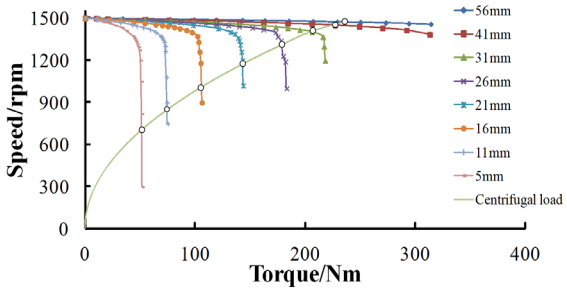

Fig. 15 Mechanical characteristic curves family and working points

According to intersection values in Fig. 15, speed regulation curve of driving centrifugal load can be obtained, as shown in Fig. 16.

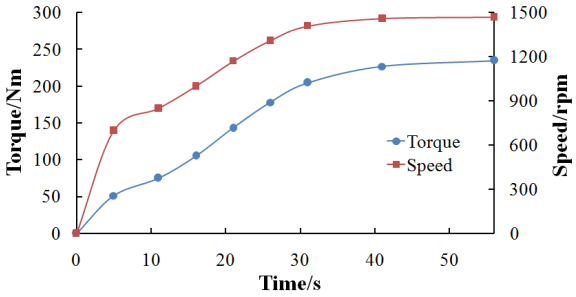

Fig. 16 Regulation curves of speed and torque

In Fig. 16, there is one to one correspondence between coupling length and output status (speed and torque). Under condition of coupling length of 30~56mm,

the curve of speed and torque is smooth, which indicates power margin of experimental prototype is sufficient.

According to Fig. 15 and Fig. 16, input power, output power and loss curves in speed regulation process can be shown in Fig. 17.

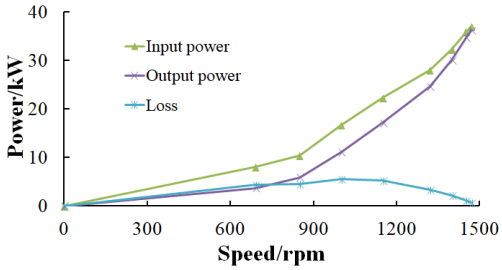

Fig. 17 Power curves in speed regulation process

In Fig. 17, the maximum loss state is 16mm coupling length and 106Nm load torque. At this time, output speed is 1000rpm and the maximum loss power is 5.55kW, which is the maximum heating spot in speed regulation process.

Taking working state of the maximum heating spot in Fig. 17 as a reference, temperature rise of each part at runtime can be detected by infrared thermometer, as shown in Fig. 18.

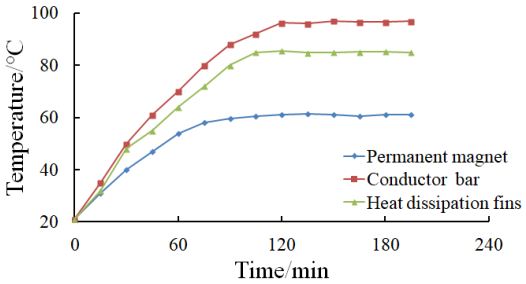

Fig. 18 Temperature rise

In Fig. 18, temperature rise curve of each part rises exponentially with time and tends to be stable after 120 minutes. Among them, stable temperature of heat dissipation fins is 85℃, stable temperature of conductor bar is 97.2℃, and final stable temperature of permanent magnet is 59℃, which is far less than the allowable maximum working temperature of permanent magnet material (120℃). Heat balance of experimental prototype is achieved under condition of the maximum heating. Compared with simulation results shown in Fig.10, stable temperature error of each part is within 10%, which further proves correctness of simulation model.

6. Conclusions

Based on rotor structure of permanent magnet synchronous motor and squirrel cage asynchronous motor, an outer cage magnetic coupling is proposed, which improves magnetic field operation efficiency, weakens eddy current loss,

and has good heat dissipation structure. The feasibility of the scheme is verified by experiments.

According to principle of equivalent magnetic circuit and equivalent circuit, electromagnetic field analysis process of outer cage magnetic coupling is simplified, and electromagnetic torque equation is deduced. The correctness of theoretical analysis is verified by experiments.

For different coupling lengths, mechanical characteristic curves family is main feature of outer cage magnetic coupling. In process of centrifugal load speed regulation, there is a one-to-one corresponding relationship between coupling length and output speed. But speed regulation process is a nonlinear slip speed regulation process, and transmission efficiency and heating are also nonlinear, the extreme point and inflection point of each characteristic curve is important reference points in design process.

Design of heat dissipation system can effectively increase heat dissipation area of experimental prototype, improve degree of air disturbance in flow field and enhance convective heat transfer capacity. The reliability of heat dissipation system is verified by simulation analysis and temperature rise experiment.

Acknowledgment

This work supported by National Natural Science Foundation of China (No. 51375063), China; Liaoning science and technology planning project (No. 2021-KF-14-05), China; Scientific research project of Liaoning Provincial Department of Education (No. LJKZ0499), China. All support is gratefully acknowledged.

REFERENCES

[1]. *Wallace A, Jouanne A V,* "Industrial Speed Control: PM Couplings an Alternative to VFDs[J]", IEEE Industry Applications Magazine, **Vol. 7**, No. 5, 2001, pp. 57-63.

[2]. *Zhao han, wang yong,tian jie, "*Review of Study on Magnet Machine and Mechchanism[J]", Chinese Journal of Mechanical Engineering, **Vol. 39**, No. 12, Dec. 2003, pp. 31-36.

[3]. *SUN Zhongsheng, Xinquan, LI Xiaoning, "*Research on Permanent Magnet Adjustable Speed Driver and Its Application[J]", Mechanical Manufacturing and Automation, **Vol. 45**, No. 03, 2016, pp. 1-4.

[4]. *He Fujun, Zhong Yuhai, Zhang Zihua, e*tc, "Research on Permanent Magnet Coupling Driving for Pumping Unit[J]", China Petroleum Machinery, **Vol. 42**, No. 10, 2014, pp. 60-64.

[5]. *Dave M P, Mokariya M K, Patel M V*, "Energy Conservation in Centrifugal Pump with Variable Frequency Drive Including SCADA, PLC and HMI[J]", International Journal of Innovative Research in Science, Engineering and Technology, **Vol. 2**, No. 5, 2013, pp. 1460-1468.

[6]. *YANG, Chaojun, GUAN Chunsong, DING Lei, LI Wenshuang,* "Transmission Characteristics of Axial Asynchronous Permanent Magnet Couplings[J]", Chinese Journal of Mechanical Engineering, **Vol.** 50, No. 01, Jan. 2014, pp. 76-84.

[7]. *Canova A, Vusini B*, "Design of Axial Eddy-Current Couplers[J]", IEEE Transactions on Industry Applications, **Vol. 39**, No. 03, Jul. 2003, pp. 725-733.

[8]. *Mohammadi S, Mirsalim M*, "Design Optimization of Double-Sided Permanent-Magnet Radial-Flux Eddy-Current Couplers[J]", Electric Power Systems Research, **Vol. 108**, Mar. 2014, pp. 282-292.

[9]. *Sun Zhongsheng, Zhou Liping, Wang Xiangdong, etc*, "Magnetic Field Analysis and Characteristics Research of Cylindrical Permanent Magnet Adjustable Speed Drive[J]", China Mechanical Engineering, **Vol. 26,** No. 13, Jul. 2015, pp. 1742-1747.

[10]. *Ge Yanjun, Yuan Zhi, Jia Feng,* "Mechanical Properties and Testing for Squirrel Cage Asynchronous[J]", Transactions of the Chinese Society of Agricultural Engineering, **Vol. 32**, No. 12, Jun. 2016, pp. 68-74.